Journal of Power Sources 214 (2012) 303–313

Contents lists available at SciVerse ScienceDirect

Journal of Power Sources

journal homepage: www.elsevier.com/locate/jpowsour

Structure-to-property relationships in fuel cell catalyst supports: Correlation of surface chemistry and morphology with oxidation resistance of carbon blacks

Kateryna Artyushkova[*,3], Svitlana Pylypenko[1,3], Madhu Dowlapalli[2,3], Plamen Atanassov[3]

Center for Emerging Energy Technologies, Chemical and Nuclear Engineering Department, University of New Mexico, Albuquerque, NM 87131, USA

HIGHLIGHTS

- Durability of modified carbon black as PEMFC catalyst supports is studied.
- Statistical structure-to-property relationship is built by PCA.
- Surface chemistry, physical properties and microscopic structure are analyzed.
- DIP of SEM images extracts roughness, texture and shape parameters.
- Wettability is a critical parameter in designing stable supports.

GRAPHICAL ABSTRACT

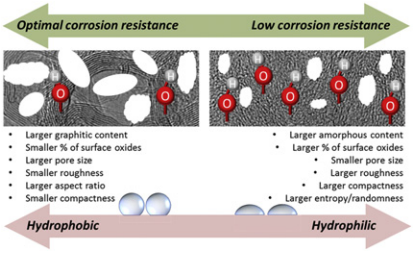

ARTICLE INFO

Article history:
Received 29 February 2012
Received in revised form
25 April 2012
Accepted 29 April 2012
Available online 3 May 2012

Keywords:
Carbon corrosion
X-ray photoelectron spectroscopy
SEM
Digital image processing
Structure-to-property relationship
Multivariate analysis

ABSTRACT

Linking durability of carbon blacks, expressed as their oxidation resistance, used in PEMFCs as catalyst supports, with their chemistry and morphology is an important task towards designing carbon blacks with desired properties. Structure-to-property relationship between surface chemistry determined by X-ray photoelectron spectroscopy (XPS), morphological structure determined by digital image processing of scanning electron microscopy (SEM) images, physical properties, and electrochemical corrosion behavior determined in an air-breathing gas-diffusion electrode is studied for several un-altered and several modified carbon blacks. We are showing that surface chemistry, graphitic content and certain physical characteristics such as Brunauer–Emmett–Teller (BET) surface area and pore volume, determined by nitrogen adsorptions are not sufficient to explain high corrosion instability of types of carbon blacks. Inclusion of morphological characteristics, such as roughness, texture and shape parameters provide for more inclusive description and therefore more complete structure-to-property correlations of corrosion behavior of carbon blacks. This paper presents the first direct statistically-derived structure-to-property relationship, developed by multivariate analysis (MVA) that links chemical and physical structural properties of the carbon blacks to their critical properties as supports for PEMFC catalysts. We have found that balance between electrocatalytic activity and high resistance towards oxidation and corrosion is achieved by balance between amount of graphitic content and surface oxide coverage, smaller overall roughness and, finally, larger amount of big elongated and loose, and, hypothetically, more hydrophobic pores.

1. Introduction

One of the main challenges in commercializing polymer electrolyte fuel cells (PEMFCs) is the need to improve their durability. Materials aspects of durability include stability of the polymer electrolyte membrane and its interfaces with the catalytic layers,

* Corresponding author.
E-mail addresses: kartyush@unm.edu (K. Artyushkova), spylypen@mines.edu (S. Pylypenko), madhud@gmail.com (M. Dowlapalli).
[1] Current Address: Materials and Metallurgical Engineering, Colorado School of Mines, Golden, CO 80401, USA. Tel.: +1 303 273 3770; fax: +1 303 273 3795.
[2] Current Address: Ascend Performance Materials, 3391 Town Point Drive Nw Kennesaw, GA 30144, USA.
[3] Tel.: +1 5052770750; fax: +1 505 2775433.

0378-7753/$ – see front matter © 2012 Elsevier B.V. All rights reserved.
doi:10.1016/j.jpowsour.2012.04.095

corrosion resistance of the micro-porous layer and the gas-diffusion layer/material, bi-polar plates corrosion, and durability of gaskets and seals. One recognized key set of durability issues in PEMFC is associated with the oxidation resistance of carbon-based support materials. It is particularly important to note that the dispersed carbonaceous materials, such as carbon blacks, employed as support for Pt-group metal (PGM) cathode catalysts are exposed to highly oxidative environment in PEMFC. They are inherently susceptible to oxidation, defined as forming of surface carbon–oxygen-containing moieties (surface oxides), that can give rise to corrosion, defined as oxidative decomposition of the carbonaceous material and its transformation (etching) with release of CO_2. A number of key properties influencing the stability of catalytic layers include the surface chemical composition and morphology, accessible surface area, electrical conductivity and pore volume, and most of these properties are associated with the properties of the carbonaceous support itself [1].

The role of carbon blacks (CB) when used as electrocatalyst support in PEMFC is to provide for anchoring of PGM nanoparticles and ensuring high surface-to-volume ratio and thus, high catalyst utilization. They also ensure electronic conductivity between the supported electrocatalyst phase and the gas-diffusing layer, usually used as current collector. The dispersion of CB's also influences mass and heat transport providing a path for even gas distribution and access to the electrocatalyst, and for the uniform removal of gas and liquid products from the catalytic layer. Surface chemistry (in particular the surface oxygen content) as well as the physical structure, the morphology, expressed through features such as roughness and compactness of pores affects hydrophobicity of the support and therefore the wetting properties with respect to products and reactants, which is critical for mass-transport properties and therefore to the overall electrode long-term functionality.

It has long been recognized that surface properties, morphology and overall structure of carbon materials strongly affect their tendency to the electrochemical corrosion (often named as "oxidation resistance"). Therefore, one of the major contributing factors to overall durability of fuel cells is the abundance of surface and bulk structural defects in the carbon-based support material. Corrosion currents typically increase with the specific surface area (usually expressed as "BET surface area") and the interlayer spacing of graphitic planes [2]. The so-called amorphous or disordered carbon, which is rich in defects, is the most prone to the attack either by the gas-phase corrosive processes (such as steam etching) or by the electrochemical oxidation. As a first step, amorphous carbon can readily react with oxygen at ambient conditions to form surface oxygen-containing groups.

During fuel cell operation, carbon blacks undergo both physical and chemical changes. Anodic oxidation of carbon blacks occurs at potentials close to those of the oxygen reduction reaction in the presence of PGM catalysts. Since graphitic carbon is more resistant to electrooxidation, carbon corrosion can be reduced by increasing the graphitic content of carbon black or specific chemical modification of carbons. The general approach to mitigation of corrosion through surface modification is to introduce functionalizing agents in the form of X–R–Y, where X is the group that reacts with the carbon black surface, R is the linking group and Y is the functional group at the carbonaceous materials interface. Different types of functionalizing agents such as sulfonates, carboxylates, tertiary amines, and steric polymers/oligomers can be used to achieve surface modification of carbon blacks to increase their oxidation resistance [3,4].

Analysis of chemical surface properties of carbons and their relationship with electrochemical corrosion has been widely studied [1,5–14]. Morphology of the support is one of the contributing factors to catalytic efficiency and stability. Also it was shown that in certain cases changes in morphology could shift the rate controlling steps of the electrode reactions and, thus, affect the overpotential. Transport behavior of gases within the support, accessibility of reactive ions to the active sites, conductivity of the support are among parameters affected by the morphology of the support which have not been studied in great detail [7]. One of the main reasons is that structural/morphological changes are not particularly easy to correlate with degradation. For the same exact reason, targeting morphological properties of materials towards those resulting in the best relevant performance characteristics is much more difficult task than changing chemistry by modifications as discussed above. It can be addressed through correlation of morphological properties resulting from particular modification or treatment of supports with performance characteristics.

There have been attempts for thorough structure-reactivity studies of the electrochemical oxidation of carbon-based materials, including very essential concept-proving studies. High-resolution transmission electron microscopy (HR-TEM), X-ray diffraction (XRD), elemental analysis, and N_2 adsorption were used to characterize different carbon support materials.[8,9]. Pore size distributions (PSD) extracted from microscopic images and adsorption data demonstrated complementary results than can be used independently to characterize porous carbons [15,16]. Direct studies of effects of morphological properties such as roughness, texture, pore size and shape parameters onto corrosion behavior and linking it back to material modification are needed to fully understand the structure-to-property correlations. Roughness as the general shape and surface irregularity is an important characteristic that affects the mass and transport behavior of the carbon blacks [17]. Penetration of gases and ions into the pores is closely related to pore size and pore shape distributions [18]. Compactness or roundness of pores affects wettability, which in turn influences transport properties of reactants within the support. The pore connectivity, which is a result of carbon particles agglomeration, and their subsequent shape parameters, also affects electrochemical properties. The relevant scale which promotes formation of an effective double-layer or the transfer of ions into the pore structure includes pores in the range of 5–100 nm. SEM is suitable to access these lateral dimensions of mesoporosity and to provide set of images representative of the morphology for statistically valid structure-to-property correlations. We have successfully demonstrated methodology for extracting quantitative morphological information from microscopic images by DIP and correlating this information with activity and durability of Pt electrocatalysts supported on some of the carbon blacks discussed herein [19].

Herein, we link surface chemical state (determined by XPS), morphological properties (determined by SEM), and electrochemical corrosion performance (determined as corrosion currents in an air-breathing gas-diffusion electrode) of several un-altered and specifically modified carbon blacks by a combination of Digital Image Processing (DIP) of SEM images and multivariate analysis (MVA). XPS was used to determine graphitic content and type and amount of carbon–oxygen specie present within the surfaces. The ability to discriminate between different carbon chemical environments, not just elemental compositions, is one of the primary advantages of XPS in the characterization of carbon-based materials. Morphological properties such as roughness, texture, porosity and shape of the pores were determined using DIP of SEM images [19]. Physical macroscopic measurements include BET surface area, pore size and pore volume. Carbon materials used in this study possess wide range of chemical and structural characteristics resulted from various chemical and temperature treatments in order to unveil direct statistical relationship between the modification, microstructure and corrosion behavior of carbon

materials. This multi-analytical approach provides a large set of parameters (structural, physical and microscopic properties), which must be related to corrosion performance. Dealing with the large number of variables (parameters), finding correlations between them and classifying samples (in this case different types of carbon blacks) is an important challenge that is addressed in this work by using multivariate statistical methods of data analysis, in particular, Principal Component Analysis (PCA) [20].

2. Experimental

2.1. Materials

As shown in Table 1, a range of samples used in this study included commercial sample of high-surface area graphitic powder (HSA_gr), several samples of untreated carbon blacks from Ketjen (KB) and Vulcan XC72 families; as well as carbon blacks modified by various undisclosed treatments provided by Cabot Corporation (Cabot SMP, Albuquerque, NM).

2.2. Instrumentation

To study carbon corrosion, an air-breathing gas-diffusion electrode has been used. This electrode was tested in a half-cell design consisting of a three-electrode system with a liquid electrolyte and a passive, air-breathing air supply. The gas-diffusion layer was initially formed by pressing 500 mg of hydrophobized (Teflonized) carbon black, such as Vulcan XC-72 modified with up to 35 wt.% Teflon, on to a nickel mesh. The nickel mesh acted as a current collector pressed within the layer of the porous hydrophobic matrix. The catalytic layer is created from a mixture of carbon blacks to be studied and hydrophobized carbon blacks (the same proportions for all types of CBs) as a binder. These are pressed on to a nickel mesh to form a working electrode. Loadings in all these experiments were maintained at 67.6 g cm^{-2}. Platinum was used as the counter electrode with $Hg/HgSO_4$ serving as the reference electrode. Polarization curves of base carbon blacks and modified carbon blacks were obtained using 2 M H_2SO_4 and their corrosion currents at 0.8 V, 1 V (approximate operating conditions of a low temperature fuel cell), 1.2 V, 1.4 V and 1.5 V for transient (current measured 15 sec after voltage is applied) and pseudo steady-state (current measured 30 min after voltage is applied) modes were measured. Since electrode surface area and loading of the material were kept the same for all samples, the comparison between samples can be performed using values of current, as measured in mA.

In the electrochemical evaluation of carbon blacks, ECSA of the working electrode is calculated for all the carbons subjected to half-cell evaluation by obtaining a cyclic voltammogram at a scan rate of 5 mV s^{-1} in the 0–200 mV range. A specific capacitance of 10 μF cm is assumed for all carbon blacks for estimating ESCA.

Table 1
Carbon black sample abbreviation and description.

Sample	Description, family
HSA_gr	Commercial HSA Graphite
KB_24	HT-Ketjen Black
HSA_XC72	HSA-Vulcan
KB_27	HT-Ketjen Black
KB_21LO	HT-Ketjen Black
HSA_XC72O	HT-HSA-Vulcan
KB_24LO	HT-Ketjen Black
KB_24L	HT-Ketjen Black
KB_27L	HT-Ketjen Black

BET surface areas were determined from nitrogen adsorption/desorption measurements performed on a Quantochrome Autosorb-I-MP instrument. The X-ray powder diffraction (XRD) patterns were obtained on a Scintag diffractometer (CuKα radiation).

XPS spectra were acquired on a Kratos Axis Ultra X-ray photoelectron spectrometer using a monochromatic Al Kα source operating at 300 W, and charge compensation using low energy electrons. The base pressure was about 2×10^{-10} torr, and operating pressure was around 2×10^{-9} torr. Three areas per sample were analyzed. Survey and high-resolution spectra were acquired at pass energies of 80 eV and 20 eV, respectively. Acquisition time for the survey and C1s spectra were 2 min and 5 min for the O1s spectra. Data analysis and quantification were performed using CasaXPS software. A linear background subtraction was used for quantification of C1s and O1s. Sensitivity factors provided by the manufacturer were utilized. All the spectra were charge-referenced to aromatic carbon at 284.7 eV. Carbon spectra were fitted with a series of 70% Gaussian/30% Lorentzian line shapes, with the exception of the graphitic component at 284.7 eV, for which asymmetric Gaussian/Lorentzian shape was utilized. The width of peaks in the curve-fit of C1s was set to be 1.0 eV [21].

SEM was performed on a Hitachi S-800 instrument. All images were acquired at the same voltage and magnification settings of 2 kV and 50 K to ensure that intensity variability in images is caused only by the variability in the morphology and not instrumental factors. SEM images from 5 different areas on the sample were acquired.

2.3. Data analysis

2.3.1. SEM images

Digital Image Processing of SEM images, including shape statistics, texture analysis, roughness and gradient analysis, was done in in-house written routine in Matlab [22] and ImageJ.

2.3.2. Multivariate analysis

Multivariate analysis of data was done using PLS_Toolbox 5.0 for Matlab [23]. Principal Component Analysis, using an autoscaling as preprocessing option (mean centering and scaling to unit variance), was the default method of data analysis.

3. Results and discussion

3.1. Electrochemical studies

For each of the carbon black samples, corrosion currents at different voltages at two conditions (transient and steady-state) were obtained. Table 2 summarizes conducted electrochemical measurements, while Fig. 1 plots corrosion currents. According to the Kinoshita-Giordano method, corrosion currents are generally represented by $i_t = kt^{-n}$ [1]. As a measure of the corrosion resistance we used Kinoshita's definition of the current at 1 V polarization, potential close to operating potential of a low temperature fuel cell, which is the largest for samples KB_24 and Vulcan HSA_XC72. Samples KB_27, KB_24L and KB_27L are the most resistant. The least resistant sample KB_24 has the highest ECSA while the most resistant sample KB_24L has low ECSA. KB_27L with its low corrosion currents at all potentials and high ECSA represents the optimal carbon support.

Electrochemical oxidation of carbon blacks in acidic electrolyte solution is a combination of two processes. Below 1.23 V carbon oxidizes to CO_2. Above 1.23 V corrosion due to oxygen evolution contributes into total corrosion current. KB_24 and HSA_XC72 are the most corrosive, while KB_24L is the most resistant samples at all potentials. The optimal carbon support sample, KB_27L, has low

Table 2
Electrochemical parameters of the corrosion behavior of the carbon blacks

	ECSA m^2	Half cell corrosion current, mA transient					Half cell corrosion current, mA steady-state				
		at 0.8 V	at 1.0 V	at 1.2 V	at 1.4 V	at 1.5 V	at 0.8 V	at 1.0 V	at 1.2 V	at 1.4 V	at 1.5 V
HSA_gr	44.5	1.07	3.60	14.2	42.8	85.1	0.18	0.77	3.7	17.1	38.3
KB_24	55.9	2.71	11.63	21.8	52.7	132.1	1.10	1.93	4.2	28.0	59.1
HSA_XC72	40.9	2.80	10.00	32.8	87.1	145.7	0.39	1.41	7.5	45.6	80.5
KB_27	43.2	0.31	0.71	3.7	14.2	58.5	0.06	0.19	1.5	10.5	27.4
KB_21LO	45.8	1.21	3.27	8.6	35.1	89.0	0.28	0.71	3.3	26.0	57.9
HSA_XC72O	45.8	1.89	4.02	10.4	34.1	97.4	0.14	0.58	3.2	33.6	76.0
KB_24LO	45.1	0.87	2.11	6.6	26.8	70.7	0.13	0.49	2.8	16.4	35.4
KB_24L	39.3	0.50	1.51	4.7	19.6	62.1	0.10	0.46	2.0	14.2	33.8
KB_27L	47.8	0.48	1.46	7.0	36.8	83.8	0.07	0.40	2.4	17.4	41.1

current at <1.2 V but pretty high currents at higher potentials due to contribution of oxygen evolution. It is important to distinguish electrochemical corrosion (below 1.23 V) from corrosion due to oxygen evolution (above 1.23 V). Though large differences and trends can be discerned from inspection of Table 2, it is hard to evaluate more in-depth similarities and differences between samples and the voltages responsible for them. In order to do so, PCA was used as analysis tool as described later in the manuscript.

Presence of Pt nanoparticles on various carbon supports as used in electrocatalysts causes increase in corrosion currents as shown in Fig. 2 for subset of carbons and electrocatalysts analyzed by us in our previous work [19]. Notably, there is no direct link between corrosive behavior of carbons and electrocatalysts, i.e. some of the less corrosive carbons result in the least corrosive electrocatalysts such as KB27L and KB24LO, but it is not the case for all carbon supports. This indicates that complete understanding of the chemistry and morphology of both carbon black supports as well electrocatalysts is critical in our ability to predict how particular type of support will behave when Pt is deposited onto it.

3.2. Physical characterization

BET surface area (*BET*), pore volume (*PV*), pore size (*PS*) obtained from N_2 adsorption/desorption measurements, and *d* spacing obtained from XRD data are reported in Table 3. The most corrosive sample HSA_XC72 has the highest BET surface area and the lowest pore size. On the other hand, the 2nd most corrosive carbon, KB_24, has opposite characteristics, i.e. the lowest BET area and the largest pore size. Generally, there is correlation between BET surface area and corrosion currents. However, KB_24 sample contradicts this well-established dependence. We will now investigate whether surface oxide functional groups may contribute to such high instability of this sample.

3.3. XPS analysis

Chemical bonding and the local structure of an atom in a compound and its electronic structure are intimately connected. This is of great importance when, as with carbon, atoms may arrange in different crystalline phases, in nanostructures, or in amorphous networks. The most stable natural forms of carbon, namely, graphite and diamond, correspond to 100% sp^2–π and 100% sp^3 hybridizations, respectively. The distribution of various types of atomic arrangements and chemical species is typically obtained *via* deconvolution of high energy resolution C 1s spectra into multiple components: carbon atoms in graphite-like environments, polyaromatic structures (the so-called aromatic peak), saturated carbon species (so-called aliphatic peak) and components for carbon atoms bonded to O and/or S atoms (e.g. C–OH, C–O and COOH).

Fig. 2 shows a subset of XPS spectra for four CB samples. Asymmetry of the peak indicates that multiple types of carbon species are present. Moreover, in photoemission spectroscopy of core levels of metals, it is accepted that the typical asymmetry towards higher binding energy is due to electron-hole pair excitations [24,25]. For graphite, when the empty density of states gradually becomes more filled, the asymmetry of the C 1s line shape increases due to the increased phase space for low-energy electron-hole pairs. This low energy continuous contribution is accounted by the asymmetric Gaussian–Lorentzian (GL) functions instead of conventionally used symmetrical GL mixture components. The width and position of asymmetric peak representing graphitic carbon was kept tightly constrained from spectrum to spectrum and extra GL peaks were added to complete the curve fit of experimental spectrum [21].

Table 4 shows results of XPS C 1s spectral deconvolution along with elemental concentration of oxygen. Small amounts of oxygen ranging from 1.9 to 5 at% are present in all samples. Range in the amount of graphitic carbon present within samples is quite large – from 44% for Vulcan to 75% for Ketjen Black. All peaks above 287 eV are summed together to represent the total amount of surface oxides C_xO_y, such as C-OH, C–OC, C–O, O–C–O, etc. The amount of surface oxides ranges from 11 to 22%. The most corrosive sample, HSA_XC72, has large amount of surface oxides and low graphitic content, and therefore exhibits low resistivity. On the other hand, another most corrosive sample, KB_24 has a small amount of

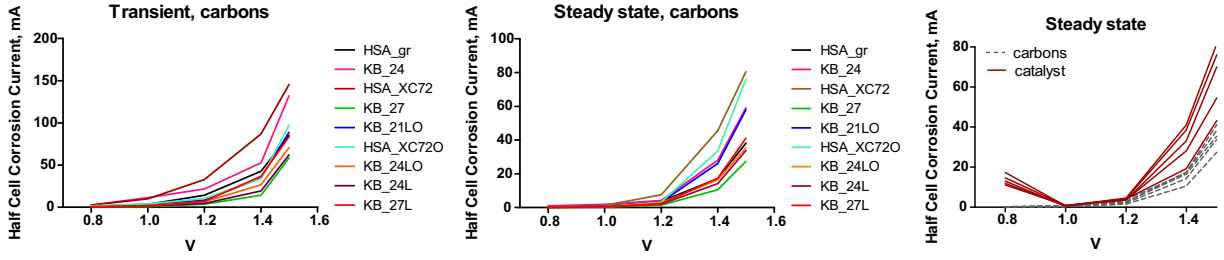

Fig. 1. Corrosion currents obtained at transient and steady-state regimes for carbons and compared for subset of carbons and catalysts for steady-state regime.

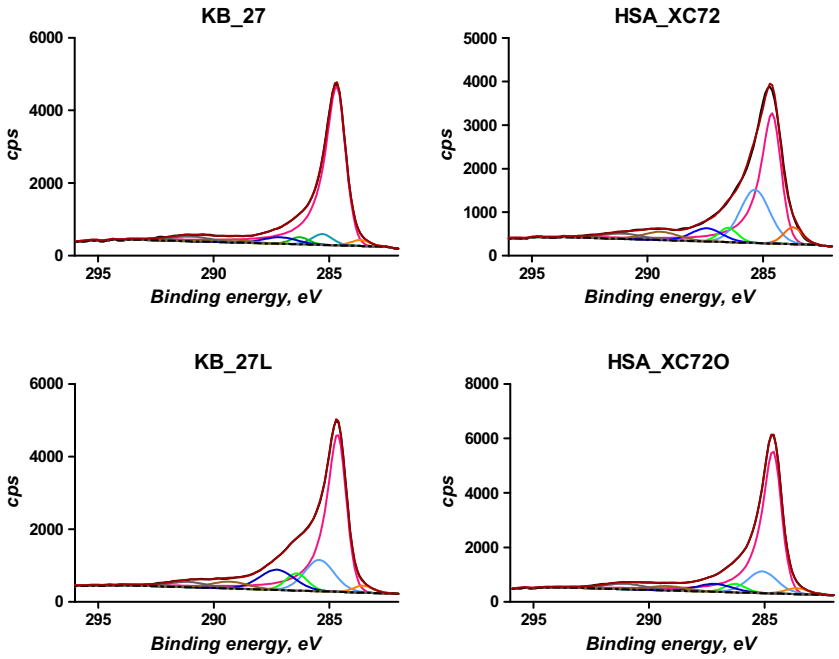

Fig. 2. High resolution C1s spectra with curve fits for four representative carbon black samples.

oxygen and high amount of graphitic carbon. In addition to physical characteristics, chemical species detected for this sample are also opposite from what is expected for carbon blacks with high affinity to corrosion. This demonstrates the need to investigate whether certain morphological characteristics are potential triggers for highly corrosive behavior of this sample.

3.4. SEM digital image processing

Representative SEM images in Fig. 3 demonstrate that with exception of graphite HSA_gr all evaluated carbon black samples have agglomerations of particles with some black areas due to open pores of various dimensions. Samples HSA_gr and KB_21LO have visible graphite planes.

One of the goals of Digital Image Processing is the conversion of 2-D images into 1-D image components that are useful for representation and description.

Surface roughness is the first order statistical parameter which is highly relevant for hydrophobicity and transport behavior of carbons [17]. The average roughness (R_a) is the arithmetic mean of the absolute values of the departure from the mean grey scale intensity. Skewness (R_{sk}) of the roughness profile describes asymmetry of the roughness, pointing to the domination of valleys (pores) or peaks in the micrograph. This parameter increases as amount of pores (dark values of intensity within images) increases.

Texture is one of the most important features used in DIP. It arises from the repetition of local patterns. Textural features, based on grey scale co-occurrence matrices (GLCM), provide measures of homogeneity, randomness or directionality [26,27]. The GLCM is a tabulation of how often different combinations of pixel intensity values (grey levels) occur in an image. The GLCM described here is used for a series of "second order" statistics calculations. Second order measures consider the relationship between groups of two (usually neighboring) pixels in the original image.

Inverse difference moment (*IDM*, also called *homogeneity*) is a measure of self-similarity, i.e. measure of probability that pixel of each region have the same values. Homogeneous images contain ideal repetitive structures, and such uniformity produces idealized patterns. Correlation (*Corr*) measures linear dependency of grey levels of neighboring pixels, with values of 0 for uncorrelated (perfectly uniform image) and 1 for perfectly correlated pixels. Angular second moment (*ASM*, also called *uniformity*) measures the orderliness of image. Higher values of ASM will be observed for more orderly images. Entropy (*Ent*) measures degree of randomness and is expected to be high when the values of the moving window have similar values. It is expected to be low when the

Table 3
Physical parameters

Sample name	Surface area, BET $m^2\ g^{-1}$	Pore vol cc g^{-1}	Pore size nm	XRD Data *d* (002) fresh
HSA_gr	315.8	0.42	8.8	3.379
KB_24	234.0	1.43	24.4	3.460
HSA_XC72	885.3	1.23	5.5	3.572
KB_27	220.0	1.50	26.7	3.429
KB_21LO	410.0	1.82	17.8	3.460
HSA_XC72O	283.0	1.32	18.8	3.465
KB_24LO	355.0	1.63	18.3	3.439
KB_24L	452.0	0.79	9.0	3.443
KB_27L	454.0	2.23	19.6	3.434

Table 4
XPS quantification results for the surface oxygen-containing species/moieties in atomic percent

Sample name	O 1s%	Carbide	C–C	C*–C–O	C_xO_y
		283.6	284.7	285.8	>287
HSA_gr	5.0	3.6	66.2	11.7	13.4
KB_24	2.2	3.3	70.8	12.4	11.4
HSA_XC72	4.2	5.6	44.2	29.6	16.3
KB_27	2.1	3.0	75.3	6.7	12.9
KB_21LO	4.0	2.6	56.2	16.9	20.3
HSA_XC72O	1.9	3.3	67.1	12.3	15.4
KB_24LO	2.9	2.9	66.3	11.2	16.7
KB_24L	3.2	3.0	63.0	13.5	17.4
KB_27L	5.1	2.8	52.5	17.6	21.9

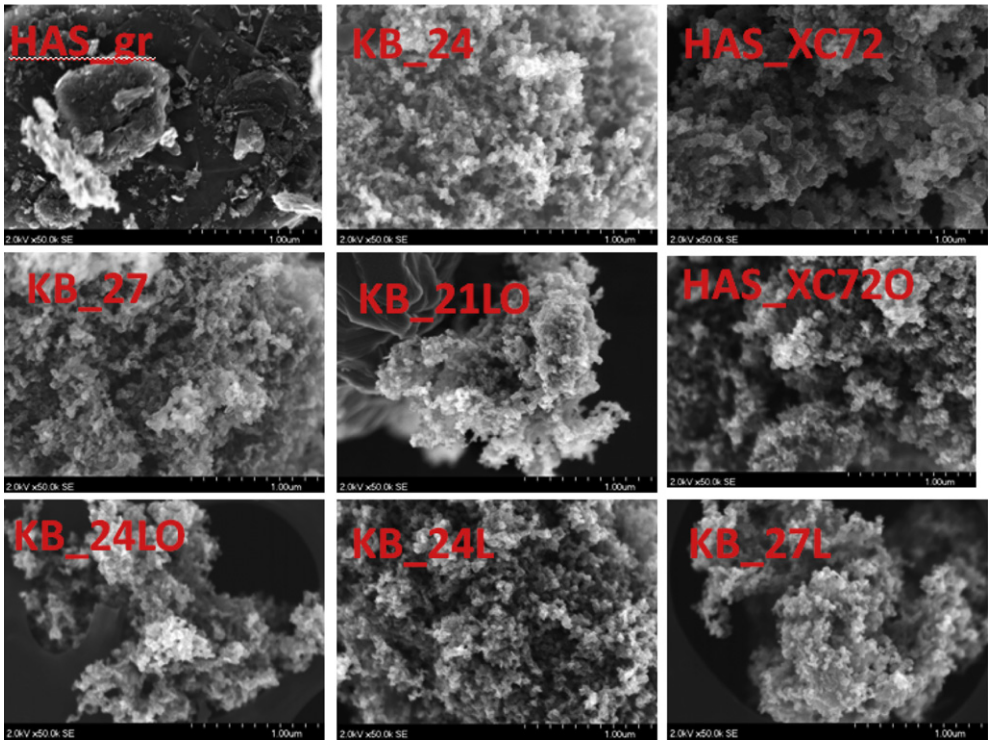

Fig. 3. SEM images of the material set of carbon blacks in this study.

values are close to either 0 or 1 (i.e. when the pixels in the local window are uniform).

Shape parameters describe the morphology such as shape, size, or orientation of pores in more details. There are dozens of shape parameters in literature that rely generally on dimensionless relations of size parameters [17,28,29]. In material engineering, the most popular is the aspect ratio *(AR)*; the ratio between the major and minor axes, representative of degree of elongation of circular pores. Compactness (*Comp*), sometimes also called shape factor, is a measure of the degree to which the shape is compact. More compactly shaped pores expected to be more wettable than loose pores, which is an important parameter in transport properties of porous materials [30].

Table 5 summarizes all statistical parameters that were extracted from images with their abbreviations and descriptions. Table 6 shows all parameters extracted for the complete set of 9 samples.

Apart from HSA_XC72, the image parameters are quite similar for all samples. Being the most corrosive sample, HSA_XC72 has the smallest R_a, average skewness R_{sk} and largest correlation. This is the sample that is the most different from all others. It exhibits highest amounts of carbides and surface oxides, largest BET and highest corrosion currents. Importantly, the 2nd most corrosive sample, KB24, for which physical characteristics and chemical surface species are opposite from the expected trend, has largest roughness and skewness, indicating rough and very porous morphology.

4. Multivariate data analysis of data from individual techniques

Major difference between samples and individual parameters responsible for those differences are obvious from visual inspection of the tables. However, it is virtually impossible to find correlations between all 28 parameters (called variables) in this way. There are 4 physical characteristics variables, 5 variables from XPS, 8 morphological parameters and 11 electrochemical characteristics. Multivariate analysis methods will be used to reduce dimensionality of the data and assist in data interpretation.

4.1. Introduction into PCA

PCA is one of the simplest multivariate statistical analysis methods, allowing for the identification of similarities and differences between samples, resulting in classification of samples into groups. At its most fundamental level, PCA visualizes the difference between samples (captured in scores) and “explains” which variables (parameters) make samples different (captured in loadings). PCA uses Singular Value Decomposition (SVD) to decompose the original data matrix into a set of new variables, called latent variables or loadings, which are a linear combination of the original measurable variables. The primary components corresponding to the largest eigenvalues represent the set of components that span significant data, while the remaining components, each describing a low variance, represent the noise in the data set. The results of PCA are usually displayed as score plots (reflecting the significance of each sample in a particular principal component), loading plots (reflecting the significance of each variable in a particular principal component) and biplots (showing both samples and variables for two principal components).

First, as an example, we will discuss interpretation of PCA results shown in Fig. 4, applied to a simple data table combining elemental composition (6 elements and 2 types of carbon) for 6 samples, shown in Table 7. The loading plot (Fig. 4b) shows the contribution of variables, while the score plot (Fig. 4c) displays the contribution of samples into Principal Component #1 (PC1). The further variables or samples are removed from the *x*-axis on the loading or score plots, the more significant they are for a given principal component. For example, O%, Mg% and carbonates% have high negative loadings into PC #1, while all other elements have positive loadings. This indicates that these two groups of variables are anticorrelated. Moreover, Cl% and Na% are located at a different

Table 5
Statistical parameters extracted from SEM images terminology.

Name of parameter (abbreviation)	Term	Description
Mean particle shape parameters		
Aspect ratio (AR)	Ratio of the objects height to its width	Minimum of 1 for a circle
Compactness (Comp)	Shape factor: 4pi × area (perimeter)	Numerical quantity representing the degree to which a shape is compact
Texture parameters		
Angular second moment (ASM)	Measure of uniformity (average certainty in grey tone co-occurrence)	Homogeneous images contain ideal repetitive structures, and such uniformity produces idealized patterns.
Correlation (Corr)	Linear dependency of grey levels of neighboring pixels	Low for perfectly uniform images, 1 for perfectly correlated pixels.
Inverse difference moment (IDM)	Measure of homogeneity, Opposite from contrast	Homogeneous images contain ideal repetitive structures, and such uniformity produces idealized patterns
Entropy (Ent)	Average uncertainty of grey tone co-occurrence, degree of randomness	High when the values of the local window have similar values. It is low when the values are close to either 0 or 1
Roughness parameters		
R_a (R_a)	Arithmetical mean deviation	Arithmetic average of the roughness profile
R_{sk} (R_{sk})	Skewness of the assessed profile	Asymmetry of the roughness profile

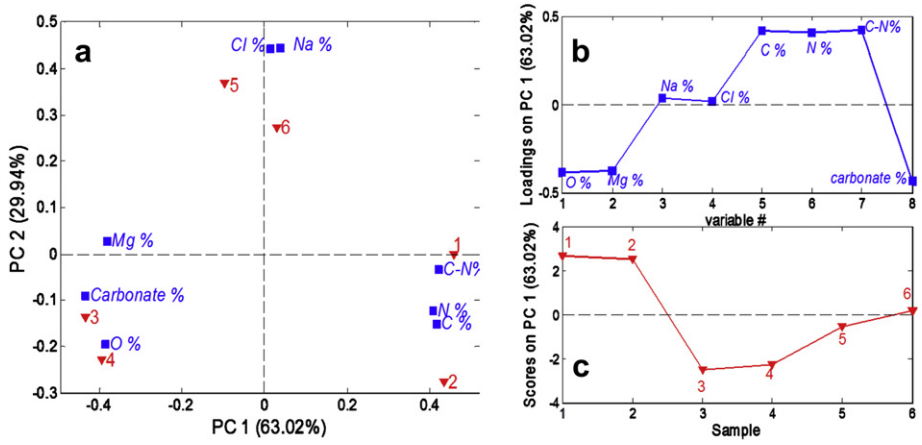

Fig. 4. PCA results from data in Table 7. Biplot (a), loading (b) and score (c) plots are shown.

distance from the zero axis than C%, N% and C–N%, reflecting the different significance of these two groups of variables into PC1. The score plot shows that samples 3 and 4 are anticorrelated with samples 1 and 2. Samples 5 and 6 are located very close to the *x*-axis, indicating that they have low contribution to this PC. By interpreting the loadings and scores plots side by side, one may conclude that samples 3 and 4 have a high contribution of O, Mg and carbonates (negative loadings and scores), while the rest of the samples have high contributions from the rest of the elements (positive loadings and scores). Values in original data table confirm these observations.

Biplots, as shown in Fig. 4a, combine the information from the scores and loadings plots. The further variables and samples from the intersection of axes, the more significant they are in describing the variability within the original data. Biplots provide a more instructive visualization of the clustering of samples for identification of variables that are the most or least important for a specific sample grouping. Correlated variables and samples will be located in the same regions of a biplot. PC1 captures 63% of variance within the data and shows the highest positive contributions from samples 1 and 2 and associated variables C%, N% and C–N%. The highest negative contributions come from samples 3 and 4 and associated Mg%, O%, and carbonates%. Samples 5 and 6 are close to zero on the *x*-axis as they have small contributions to PC1. It means that both groups of variables with high positive and high negative contribution into PC1, equally contribute into the composition of samples

Table 6
Statistical parameters extracted from SEM images.

	HSA_gr	KB_24	HSA_XC72	KB_27	KB_21LO	HSA_XC72O	KB_24LO	KB_24L	KB_27L
ASM	6.0E-04	6.5E-04	2.0E-04	6.0E-04	4.6E-04	8.9E-04	7.5E-04	5.0E-04	6.1E-04
Corr	3.7E-04	6.3E-04	8.2E-04	8.0E-04	4.3E-04	5.2E-04	4.3E-04	5.4E-04	7.3E-04
IDM	0.26	0.31	0.09	0.29	0.29	0.37	0.39	0.28	0.31
Ent	8.16	7.81	8.96	7.80	8.18	7.63	7.78	8.06	7.80
Comp	0.82	0.79	0.78	0.81	0.84	0.83	0.82	0.80	0.82
AR	1.67	1.80	1.82	1.71	1.57	1.63	1.64	1.72	1.69
R_a	41.6	41.9	26.0	29.0	36.4	35.1	37.2	35.2	29.6
R_{sk}	1.11	0.77	0.43	0.36	0.06	0.82	0.43	0.49	0.03

Table 7
Elemental quantification of 6 samples using XPS.

Sample	O 1s	Mg 2p	Na 1s	Cl 2p	C 1s	N 1s	C 286.5 eV	C 290 eV
1	32.7	4.5	8.0	4.1	42.5	3.3	37.8	15.4
2	33.5	5.9	2.0	1.3	46.5	4.9	29.7	15.9
3	48.8	10.1	4.5	2	23.4	0.8	13.5	52.1
4	54.6	7.4	2.2	1.9	26.4	0.4	9.1	49.2
5	37.2	7.3	13.3	8.6	24.8	1.4	14.5	31.3
6	33.6	7.9	12.6	6.5	31.4	1.5	21.0	25.0

5 and 6. In other words, amounts of C, N, Mg, O, C—N, and carbonates for samples 5 and 6 are close to the average amounts of these species for all samples. These samples, however, have the highest positive contribution into PC2, which captures 23% of variance in the data, due to higher than average amounts of Na% and Cl%. As a result, three distinct groups of samples are represented on the biplot for the example shown in Fig. 4. Samples 1 and 2 have a high contribution from an organic phase, which includes C, N, and C—N species; samples 5 and 6 are enriched in salt (Na and Cl) and samples 3 and 4 are enriched in a metal carbonate phase (O, Mg and carbonates). The function of PCA in this type of analysis is to find samples which are globally correlated or anti-correlated, and to facilitate visualization of the variables responsible for the correlations. Such use of biplot will be applied herein to simplify association of variables from multiple techniques for various samples.

4.2. Classification of samples based on corrosion current

Fig. 5 shows PCA results applied to corrosion currents in transient and steady-state conditions. PC1 separates samples based on the corrosion currents. All variable based on current measurements contribute positively into PC1, which captures ~83% of variance within the data. Samples that have high positive loadings, such as XC_72 and KB_24, are highly corrosive, while samples which have negative loading into PC1 (i.e. KB_27, KB24L, etc) are the least corrosive. PC2 captures ~11% of variance in the data and separates samples based on electrochemical corrosion (currents up to 1.3 V) and corrosion due to evolution of oxygen (above 1.3 V). Corrosion properties of the most corrosive samples XC_72 and KB_24 are quite different. KB24 has higher currents due to electrochemical corrosion (at potentials upto 1.23 V), while XC_72 has higher currents due to contribution of corrosion from oxygen evolution (at potentials higher than 1.23 V).

4.3. Classification of samples based on surface chemistry

Fig. 6 shows PCA results applied to Table 4. PC1 captures ~63% of variance in data and reflects domination of surface oxides (positive loadings) versus graphitic carbon (negative loadings). Vulcan XC72 is the most different CB from all others, having the highest positive loading into PC1, as it has highest amounts of oxygen, surface oxides and carbides. This sample was among the two most corrosive separated by PCA applied to corrosion currents (Fig. 5) largely due to evolution of oxygen. Ketjen black modified samples, KB_21LO and KB_27L, also have high amounts of oxygen and surface oxides, but they show high corrosion resistance. Samples on the left part of biplot, having negative loadings in PC1, have high contribution of graphitic carbon. Samples in between that are close to zero *x*-axis (HSA_gr and KB_24L), have equal contribution from graphitic carbon and surface oxides. Sample KB24, which is also among most corrosive ones at lower potentials (electrochemical corrosion), falls into the group with other not corrosive samples having large amounts of graphitic carbon and low amounts of surface oxides. Side by side comparison of Figs. 5 and 6 clearly visualizes that chemical surface composition is not major stand-alone factor that determines durability of carbon blacks.

5. Structure-to-property relationship

For direct structure-to-property correlations, data from all characterization methods were combined into one dataset and PCA was applied.

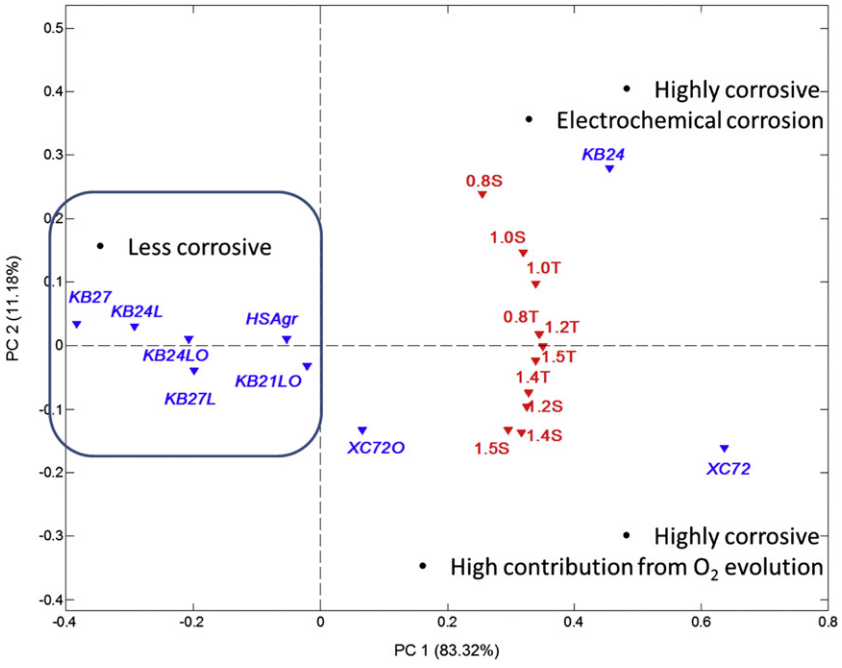

Fig. 5. PCA results from corrosion data in Table 2. PC1 separates samples by more/less corrosive. PC2 separates samples by type of corrosion.

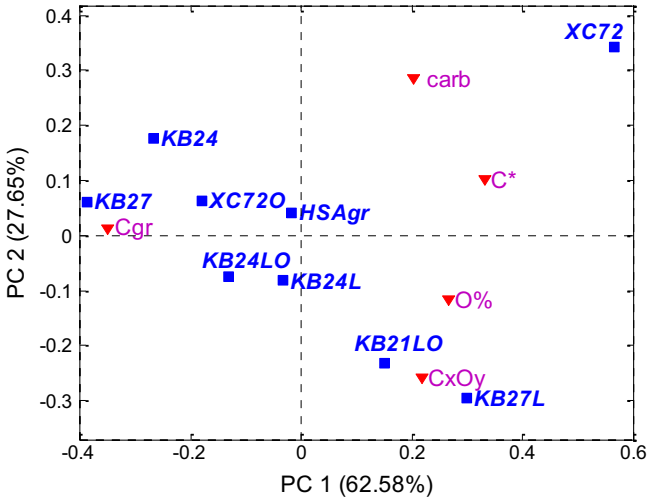

Fig. 6. PCA results applied to XPS quantification results in Fig. 4.

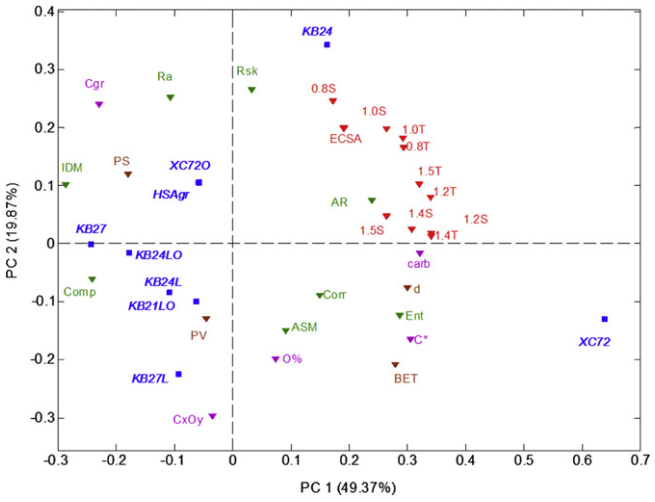

Fig. 8. PCA results to table combining all data for all samples.

First, we analyze correlation between physical, compositional and electrochemical parameters discussed above, as these relationships are of most interest during designing optimal carbon support. Fig. 7 shows PCA biplot for this set of parameters.

High corrosion currents do correlate with large *BET* area, large *d* spacing, presence of large amount of oxygen and low amount of graphitic carbons, which conforms with conventional understanding of characteristics causing low durability. Large pore size and pore volume is typical for samples with higher amount of graphitic carbon resulting in lower corrosion currents. Importantly, however, the 2nd most corrosive sample KB24 stands away on the biplot from parameters identified as highly significant for instability. Corrosion behavior of this sample is, thus, different from that of XC72 sample and cannot be explained by surface chemistry and physical characteristics alone. Therefore, influence of morphological parameters which play crucial role in corrosion kinetics is studied next.

All data available were combined into one data table and PCA was applied (Fig. 8). Similar to results from corrosion data themselves (Fig. 5), positive loadings of all values of current into PC1 indicate samples which are high in corrosion, i.e. (XC72 and KB24), and negative values of loading show samples which are low in corrosion. Skewness R_{sk} which is indicator of number of pores and large *AR* have high contribution to sample KB24, while large *BET*, *entropy*, *correlation* and *ASM* have high significance for XC_72. More heterogeneous morphology with lots of elongated pores results in higher electrochemical corrosion currents at lower voltages, while more uniform random morphology with smaller roughness but larger BET surface area results in corrosion currents at higher voltages due to evolution of oxygen. More homogeneous and uniform morphologies with large overall roughness and large pores and pore volume result in better corrosion resistance.

With XC_72 being so different from all the other samples in having highest currents due to evolution of oxygen, it was also important to study structure-to-property correlations with this sample excluded from the model to highlight the effect of electrochemical corrosion. Results of PCA applied to the rest of samples are shown in Fig. 9.

Samples XC72O, HSAgr and KB24 are the most corrosive and have highest ECSA, overall roughness R_a, skewness R_{sk}, d-spacing and aspect ratio *AR*. Samples KB27L and KB21LO are also somewhat

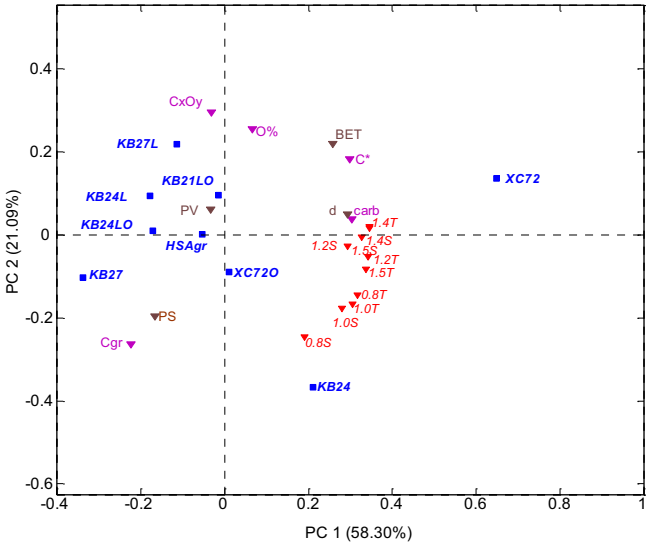

Fig. 7. PCA results to table combining physical, XPS and corrosion currents for all samples.

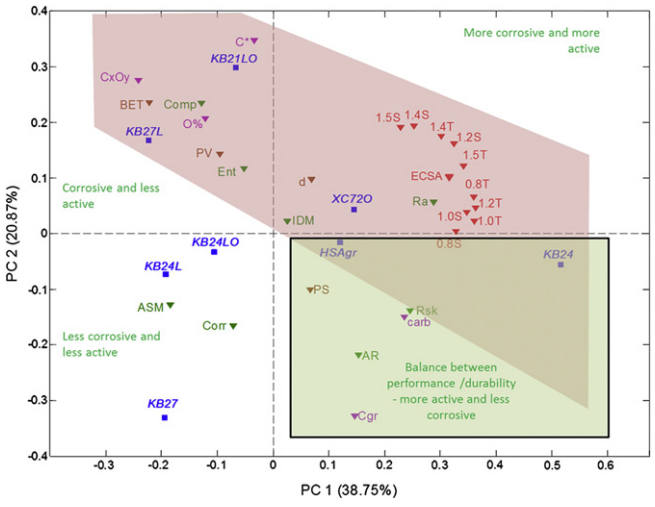

Fig. 9. PCA results to table combining all data, sample XC-72 is excluded.

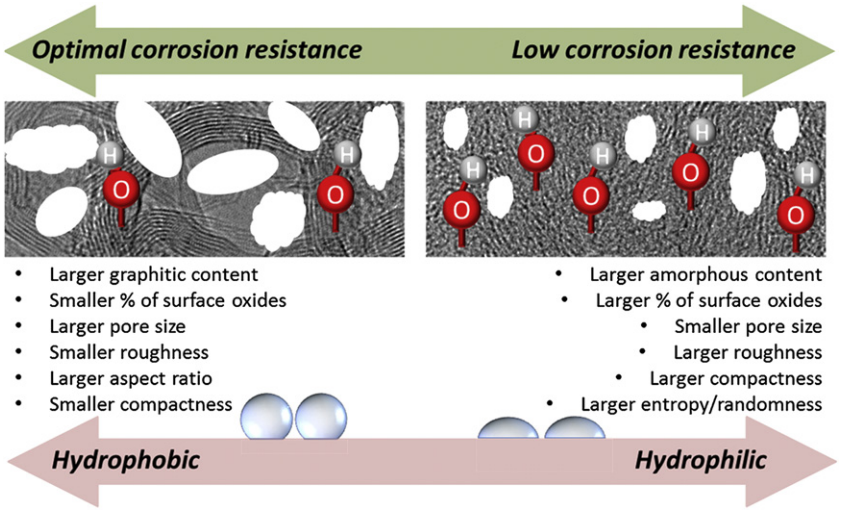

Fig. 10. Structure-to-property relationship for carbon black samples with optimal and low corrosion resistance.

corrosive, as captured by PC 2, and they have the highest amount of surface oxides, which correlates with large *BET* and *Pore Volume*, *entropy* and *compactness*.

Samples KB24L, KB24LO and KB27 contributing negatively into both PCs are the least corrosive but also potentially least active based on ECSA. The subquadrant on PC biplot containing samples with positive loading into PC1 and negative loading into PC2 is where the samples with optimal properties would be located. Moderate ECSA and moderate corrosion stability would make them ideal. None of the pristine and modified samples studied herein fall into this category. Such ideal samples should have the highest amounts of graphitic carbon, largest pore size *PS* and R_{sk}, which is representative of the amount of pores, and larger aspect ratio *AR* and smallest *compactness*.

Structure-to-property correlation analysis indicates that carbon black samples with large *BET*, heterogeneous (R_a), randomly oriented (*Entr*), compact (*Comp*) smaller pores (*PS*) and large amount of surface oxides (C_xO_y, *O%*) content result in high corrosive behavior. All of these parameters represent supports with high wettability of pores, which may be the parameter that needs to be investigated in more details when designing carbon-based supports for Pt-based electrocatalysts. Carbon blacks possessing more homogeneous morphology with large amount (R_{sk}) of elongated pores (*AR*) and not as high roughness (R_a), large pore size (*PS*) and high graphitic carbon (*Cgr*) content are less corrosive and at the same time potentially more electrochemically active. Fig. 10 summarizes the vision behind discovered relationship between chemical structure, morphology and electrochemical properties of carbon blacks.

6. Conclusions

A multi-analytical approach combining surface analysis using XPS, microscopic analysis using SEM imaging, physical macroscopic characterization and electrochemical evaluation of carbon blacks was performed to provide comprehensive understanding of carbon black structure and morphology. Digital Image Processing (DIP) was applied to SEM images to extract texture, shape, and roughness statistics. PCA was used as the main visualization tool to elucidate statistical correlations among various properties.

Samples with the highest potential activity for oxygen reduction reaction and highest corrosion were found to have high surface area, high roughness and large amounts of surface oxides. Samples with moderate activity and high resistance towards corrosion have large amounts of graphitic carbons and large amount of large not very compact elongated pores. All of these parameters represent supports with high hydrophobicity, which may be the parameter that needs to be investigated in more details when designing carbon-based supports for Pt-based electrocatalysts. Identification of properties of the sample that matches optimal surface chemical and morphological composition can serve as guidance in type of modifications that must be performed.

Acknowledgements

We would like to acknowledge the support of DOE-EPSCoR DE-FG02-08ER46530 New Mexico Implementation Program.

References

[1] K. Kinoshita, J. Bett, Carbon 11 (1973) 237–247.
[2] P. Stonehart, Carbon 22 (1984) 423–431.
[3] D. Belanger, M. Toupin, J. Phys. Chem. C 111 (2007) 5394–5401.
[4] X.K. Wang, D.D. Shao, Z.Q. Jiang, Plasma Process. Polym. 7 (2010) 552–560.
[5] P.L. Antonucci, L. Pino, N. Giordano, G. Pinna, Mater. Chem. Phys. 21 (1989) 495–506.
[6] A.S. Arico, V. Antonucci, M. Minutoli, N. Giordano, Carbon 27 (1989) 337–347.
[7] R. Borup, J. Meyers, B. Pivovar, Y.S. Kim, R. Mukundan, N. Garland, D. Myers, M. Wilson, F. Garzon, D. Wood, P. Zelenay, K. More, K. Stroh, T. Zawodzinski, J. Boncella, J.E. McGrath, M. Inaba, K. Miyatake, M. Hori, K. Ota, Z. Ogumi, S. Miyata, A. Nishikata, Z. Siroma, Y. Uchimoto, K. Yasuda, K.I. Kimijima, N. Iwashita, Chem. Rev. 107 (2007) 3904–3951.
[8] O.V. Cherstiouk, A.N. Simonov, N.S. Moseva, S.V. Cherepanova, P.A. Simonov, V.I. Zaikovskii, E.R. Savinova, Electrochim. Acta 55 (2010) 8453–8460.
[9] K.G. Gallagher, G. Yushin, T.F. Fuller, J. Electrochem. Soc. 157 (2010) B820–B830.
[10] N. Giordano, P.L. Antonucci, E. Passalacqua, L. Pino, A.S. Arico, K. Kinoshita, Electrochim. Acta 36 (1991) 1931–1935.
[11] K. Horita, Y. Nishibori, T. Ohshima, Carbon 34 (1996) 217–222.
[12] R.O. Loutfy, Carbon 24 (1986) 127–130.
[13] A.B. Palotas, L.C. Rainey, A.F. Sarofim, J.B. VanderSande, P. Ciambelli, Energy Fuels 10 (1996) 254–259.
[14] F. Rositani, P.L. Antonucci, M. Minutoli, N. Giordano, Carbon 25 (1987) 325–332.
[15] Z.H. Huang, F.Y. Kang, W.L. Huang, J.B. Yang, K.M. Liang, M.L. Cui, Z.Y. Chen, J. Colloid. Interface. Sci. 249 (2002) 453–457.
[16] D. Lozano-Castello, D. Cazorla-Amoros, A. Linares-Solano, K. Oshida, T. Miyazaki, Y.J. Kim, T. Hayashi, M. Endo, J. Phys. Chem. B 109 (2005) 15032–15036.
[17] K.A. Alshibli, M.I. Alsaleh, J. Comput. Civil Eng. 18 (2004) 36–45.
[18] S.I. Pyun, C.K. Rhee, Electrochim. Acta 49 (2004) 4171–4180.
[19] K. Artyushkova, S. Pylypenko, M. Dowlapalli, P. Atanassov, RSC Advances, available online (2012).
[20] J.E. Fulghum, K. Artyushkova, Abstr. Pap. Am. Chem. S. 236 (2008).
[21] J. Walton, P. Wincott, N. Fairley, A. Carrick, in: Acolyte Science, 2010.

[22] K. Artyushkova, GUI for calculating 1st and 2nd order statistics from images, http://bit.ly/aqel66.
[23] PLS Toolbox 5.0, Eigenvector Research Inc, Wenatchee, WA.
[24] G. Speranza, L. Minati, M. Anderle, J. Appl. Phys. 102 (2007).
[25] P. Bennich, C. Puglia, P.A. Bruhwiler, A. Nilsson, A.J. Maxwell, A. Sandell, N. Martensson, P. Rudolf, Phys. Rev. B 59 (1999) 8292–8304.
[26] R.B. VonDreele, J. Appl. Crystallogr. 30 (1997) 517–525.
[27] J.-P.D. Costa, C. Germain, P. Baylou, in: 2001-GRETSI – Actes de Colloques, 2001.
[28] H. Mamane, C. Kohn, A. Adin, Separ. Sci. Technol. 43 (2008) 1737–1753.
[29] M. Tanaka, Y. Kimura, R. Kato, N. Oyama, J. Mater. Sci. 40 (2005) 2583–2585.
[30] R. Cucchiella, G. Falini, M. Ferri, M. Stracquadanio, C. Trombini, J. Environ. Monit. 11 (2009) 181–186.